Preparation and Electrochemical Characterization of Anatase Nanorods for Lithium-Inserting Electrode Material

Xueping Gao,*,† Huaiyong Zhu,‡ Guiling Pan,† Shihai Ye,† Ying Lan,† Feng Wu,†,§ and Deying Song†

Institute of New Energy Chemistry Material, Nankai University, Tianjin 300071, China, Electron Microscope Unit and School of Chemistry, The University of Sydney, NSW 2006, Australia, and School of Chemical Engineering and Environmental, Beijing Institute of Technology, Beijing 100081, China

Received: September 20, 2003; In Final Form: November 24, 2003

The titanium oxides with one-dimensional (1D) nanostructure are of significance in electrochemical lithium insertion owing to their high specific surface area and pore volume. In this study, nanorods with diameters of ca. 3−5 nm and lengths of 40−60 nm were prepared through the hydrothermal treatment of a hydrolysate obtained from $TiCl_4$ with caustic soda as demonstrated by HRTEM. These nanorods are protonated titanate and can be converted into the anatase (TiO_2) nanorods by a calcination at 400 °C. The anatase nanorods have a large specific surface area of 314 m^2/g and a high pore volume of 1.514 cm^3/g, respectively. The anatase TiO_2 nanorods exhibit a large initial electrochemical lithium insertion capacity of 206 mAh/g and good reversibility. The splitting and multi peaks in cyclic voltammograms associated with differing site occupations are ascribed to the formation of the imperfection of the TiO_2 nanorod lattice, which facilitates the transport of lithium in surface defects and bulk materials.

I. Introduction

Metal oxide nanocrystallites with morphological specificity on a nanometer scale are very attractive advanced materials because of their superior physicochemical properties and potential application as catalysts, sorption media, nanoelectronic devices, solar energy converting, and energy storage materials. For instance, nanostructured anatase TiO_2 has been recently emphasized as a material for electrochemical lithium insertion[1,2] and photocatalytic reaction.[3] The titanium oxides with one-dimensional (1D) nanostructures are of particular significance because the unique morphology brings several important features. It allows very large specific surface area and pore volume; the dimensions in the two directions perpendicular to long axis of the particles are comparable to the mean-free-path length of electrons,[4] and they can be readily separated from a suspension after a reaction. A number of preparation methods of nanostructured TiO_2 have been recently reported, such as treating TiO_2 powders in NaOH solution, and using porous anodic alumina as a template to obtain TiO_2 nanoribbons,[5] nanowires,[6] and nanotubes.[7−11] The hydrothermal synthesis of 1D nanostructured TiO_2 with NaOH solution shows a potential advantage in quantity in fulfilling the requirements as electrode materials. It is also noted that the structures of the 1D nanostructured TiO_2 products could be markedly dependent on the starting TiO_2 materials. Nanotubes with outer diameters between 10 and 20 nm are obtained by the hydrothermal synthesis when starting with titania powder of relative large particle size, such as rutile TiO_2, Degussa TiO_2 (P25), and SiO_2-TiO_2 mixture.[7−8] This feature can be utilized to tailor the structural properties of 1D nanostructured TiO_2 product. For electrode materials, particulates with a large specific surface area (and thus smaller diameter of the 1D nanostructure) are generally desirable. The sizes in two dimensions of the 1D-particles are small, which will facilitate the diffusion of lithium ions into the TiO_2.

In this study, titanate nanorods with diameters of ca. 3−5 nm and lengths of 40−60 nm were prepared through a soft chemistry route and converted into TiO_2 nanorods in a subsequent heating. It is known that cations can be inserted into protonated titanates of layered structures.[12] The TiO_2 nanorods derived from such protonated titanates could retain such a property. The electrochemical insertion of lithium into the anatase TiO_2 nanorods thus obtained was investigated by cyclic voltammetry and a galvanostatic method.

II. Experimental Section

1. Materials Used. $TiCl_4$ was analytic grade supplied by ABC (cautions should be taken on dealing with this chemical because of the severe hydrolysis in air). Analytical grade NaOH pellets (corrosive!) from ABC were used.

2. Sample Preparation. Fresh amorphous hydrolysate was prepared from $TiCl_4$ (as described in reference 13) and mixed with 15 M NaOH solution while being stirred magnetically. The mixture was then autoclaved at 110 °C for 48 h. The solids in the mixture were recovered, and rinsed first with deionized water, then neutralized with 0.1 M HCl solution. Finally they were washed with deionized water until a pH value of about 7 was reached. The washed samples were dried at 110 °C for 1 day and then calcined at 400 °C for 3 h in air. The titanium in $TiCl_4$ was almost transferred to final products with a small loss during the washing process. The production yield of the samples was over 90%.

3. Sample Characterization. Transmission electron microscopy (TEM) images were taken with a JEOL 4010 microscope

* Corresponding author. Tel: +86-22-23500876. Fax: +86-22-23502604. E-mail: xpgao@nankai.edu.cn.
† Nankai University.
‡ The University of Sydney.
§ Beijing Institute of Technology.

10.1021/jp036821i CCC: $27.50
Published on Web 02/07/2004

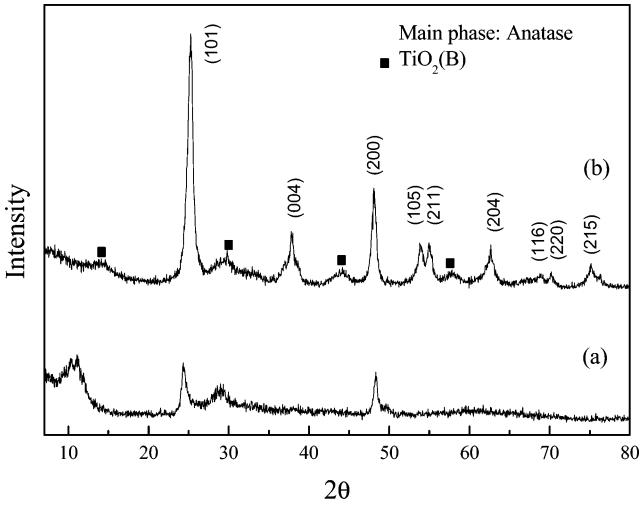

Figure 1. XRD patterns of samples: (a) as-prepared, and (b) after calcinations at 400 °C.

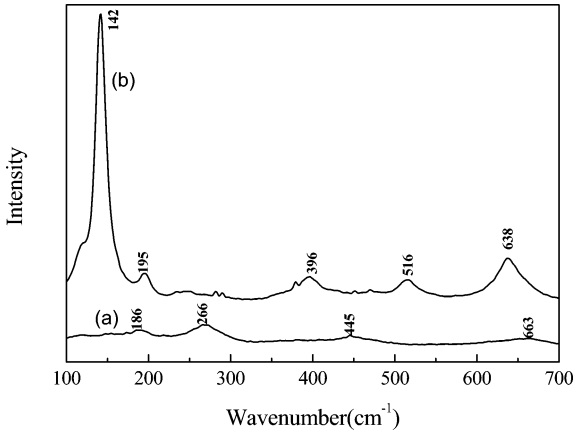

Figure 2. Raman spectra of samples: (a) as-prepared, and (b) after calcinations at 400 °C.

on powder samples deposited onto a copper micro-grid coated with holey carbon. An accelerating voltage of 400 kV was used. X-ray diffraction (XRD) patterns of sample powder were recorded on a Rigaku D/max-2500 X-ray diffractiometer equipped with a graphite monochromator. Cu K_α radiation and a fixed power source (40 kV, 40 mA) were used. The scan rate was 1 degree (2θ)/min. N_2 adsorption/desorption isotherms were measured at liquid nitrogen temperature using Autosorb-1 (Quantachrome). The samples were degassed at 250 °C and a vacuum below 10^{-3} Torr for 16 h prior to the measurement. The specific surface area, pore volume, and pore size distribution of the samples were calculated from the nitrogen sorption data. The Raman spectra of the samples were recorded by a laser Raman scattering spectrometer (Spex-1403) at the output power of 100 mW and laser wavelength of 488 nm.

4. Electrochemical Lithium Insertion. The working electrode was prepared by compressing a mixture of the active materials, conductive material (acetylene black), and binder (PTFE) in a weight ratio of 85/10/5. Lithium metal was used as the counter and reference electrodes. The electrolyte was 1 M of $LiPF_6$ in a 6/3/1 mixture of ethylene carbonate (EC), propylene carbonate (PC), and dimethyl carbonate (DMC). The galvanostatic method at discharge−charge current density of 50mA/g was used to measure the electrochemical capacity of the electrode at 20 °C. The cyclic voltammetry (CV) experiment was conducted at a scan rate of 0.2 mV/s using a Solartron 1287 potentiostat.

III. Results and Discussion

The powder XRD patterns of as-prepared and calcined samples are given in Figure 1. All peaks in the XRD patterns of the as-prepared samples can be indexed as the layered protonated titanates with monoclinic structure. After the calcination at 400 °C for 3 h, the main phase is anatase phase, and the coexisting residual phase of ca. 12−14% is the TiO_2(B) (JCPDS 35-0088) with monoclinic structure. It is reported that TiO_2(B) slowly converted into anatase at temperatures between 600 and 700 °C.[14] However, the sintering and growth of the nanorods were observed over 500 °C, resulting in serious loss of the original morphology. Thus, in this work 400 °C was chosen as calcination temperature in order to remove water and maintain the unique morphology of nanorods (as shown in Figure 3) although a small amount of coexisting TiO_2(B) was found.

The crystalline sizes of the as-prepared and calcined TiO_2 samples were estimated from XRD patterns using Sherrer's equation with their (101) peaks, being 7.7 and 9.0 nm, respectively. The result of XRD analysis is supported by the Raman spectra of the samples, which were shown in Figure 2. The spectrum for the calcined sample has absorption bands with relatively stronger intensity at 142, 195, 396, 516, and 638 cm^{-1}, being in good agreement with the typical Raman spectrum of the anatase phase.[15−16] However, the observed Raman peaks of the as-prepared samples with lower intensity can hardly be assigned to definite vibration modes. Thermal gravimetrical analysis (TGA) indicates a mass loss of about 13 wt % before 400 °C, and this is attributed to the loss of water from the sample. Therefore, the solid before the calcination is deduced to be titanate hydrate $H_2Ti_3O_7 \cdot H_2O$, which is also demonstrated in layered trititanate nanotubes.[17−18] We also found that the 101 peak in the XRD pattern of the titanate shifts to a lower angle, after a treatment with an aqueous solution of tetrabutylammonium (TBA). Layered protonated titanate structure swelled in the TBA solution,[12] and this could result in the observed peak shift.

The results of HRTEM and nitrogen sorption indicate that the nanorod morphology was retained during the calcinations at 400 °C. The TEM and HRTEM images of the titanate (as-prepared) and anatase (calcined) samples are illustrated in Figure 3. One can see clearly a large quantity of the thin nanorods with a uniform size, although the purity of the nanorods is difficult to describe accurately from only the TEM image of calcined samples (Figure 3b). These nanorods are about 3−5 nm thick and 40∼60 nm long, being markedly smaller than the nanotubes and nanoribbons reported in the literature.[6−8] The BET surface area and pore volume of the titanate nanorods are 385 m^2/g and 1.444 cm^3/g, respectively. The large pore volume should be attributed to the inter-rod voids of the randomly stacked thin nanorods, according to pore size distribution derived from N_2 sorption data. After calcinations at 400 °C, the sample is converted to the anatase phase from protonated titanate but retains the nanorod morphology (Figure 3b) and a relative large surface area of 314 m^2/g. It appears that at 400 °C a slight particulate sintering occurs, causing a small decrease in surface area. Moreover, the anatase nanorods have an even larger pore volume (1.514 cm^3/g). The increase in the pore volume caused by the calcinations is mainly attributed to the dehydration and crystallization of the nanorods, as indicated by TGA experiment. The large pore volume is favored for transportation of the species participating in the reaction on the rod surface. The interplanar spacing of the anatase rods is calculated to be ca. 0.35 nm, which corresponds to the crystalline axis oriented along the [100] direction as found in TiO_2 nanoparticles.[19] In addition,

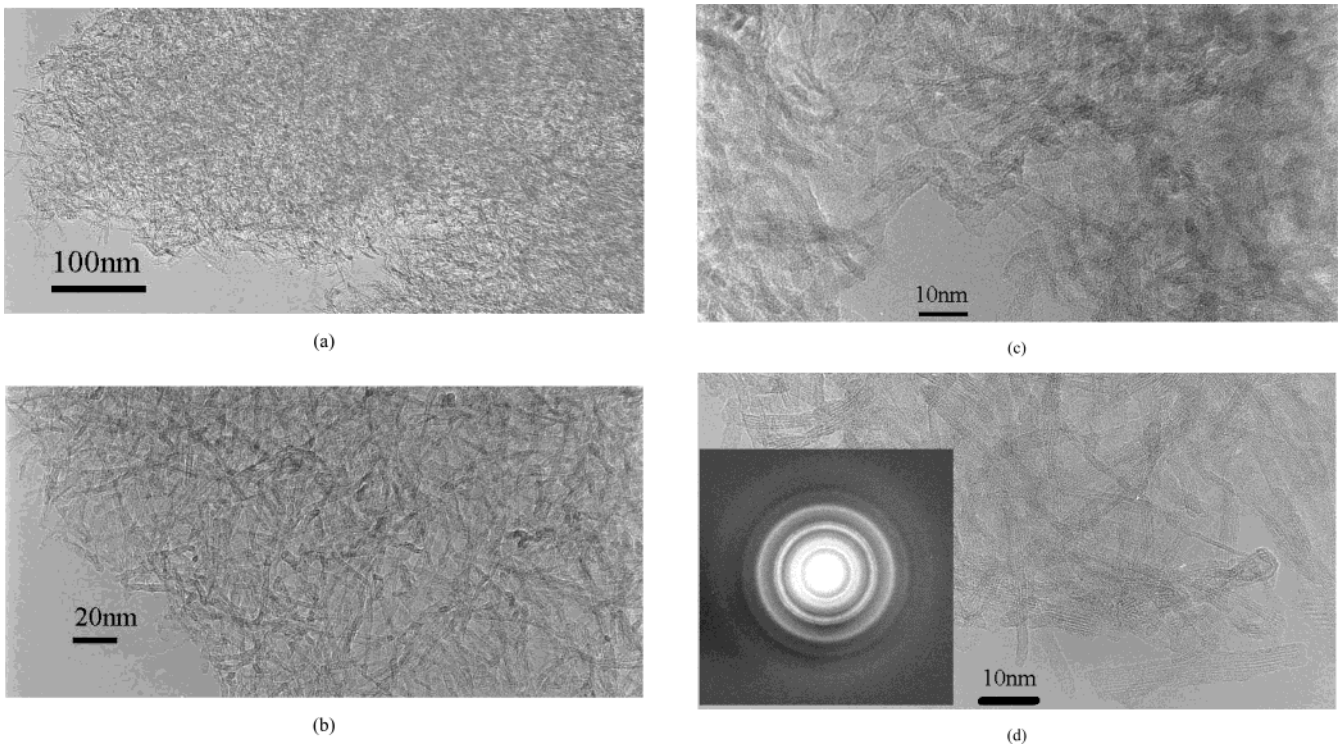

Figure 3. TEM and HRTEM images of samples: (a, c) as-prepared, and (b, d) after calcinations at 400 °C. Selected-area electron diffraction (SAED) pattern from the calcined sample is inserted in Figure 3d.

ring patterns are observed in a selected area of electron diffraction (SAED) of the calcined nanorods as inserted in Figure 3c, which are (101), (004), (200), and (105) diffractions of the polycrystals or nanocrystals of the anatase phase, similar to TiO_2 nanotube.[7,20]

It is clear, according to the analysis of the XRD patterns, Raman spectra and TEM images, that the nanorods of polycrystalline anatase resulted from titanate nanorods during the calcinations. Nevertheless, the formation mechanism of the nanorods has not been completely understood at this stage. Yao et al.[21] found that a higher temperature (higher than 90 °C) provides a strong driving force for rolling up the anatase sheets, and thus results in a nanotube structure. Amorphous TiO_2 raw materials did not form sheets under the same hydrothermal condition. However, it is recognized that the reactant, the freshly amorphous hydrolysate material, appears to be a crucial issue in the hydrothermal treatment with concentrated caustic soda. The large particulates of titania, such as rutile TiO_2, Degussa TiO_2, and SiO_2-TiO_2 mixture, yield nanotubes with an outer diameter between 10 and 20 nm through a treatment with NaOH solution.[7−8]

The results of this study also suggest a surprising fact that layered protonated titanates can be synthesized at a temperature as low as 110 °C and in aqueous solution. Titanates are usually prepared by heating a mixture of alkali carbonate and titanium dioxide at a temperature above 800 °C, followed by a treatment with mineral acid solution. Obviously, the pyro-reaction produces large particles only rather than particles on a nanometer scale. As the TiO_2 nanorods obtained in this study are only a few nanometers in thickness, it is of significant advantage. The thickness is comparable to the mean-free-path length of electrons so when excited by irradiation the electrons in the rods have a high chance to reach the rod surface, and Li^+ ions can readily diffuse into the rods from outside. In addition, the rods have a large specific surface area and pore volume. Therefore, they have a great potential for applications as industrial catalysts for desulfuration, photoassistant for oxidation or reduction of organic pollutants, and electrode materials of rechargeable lithium ion batteries.

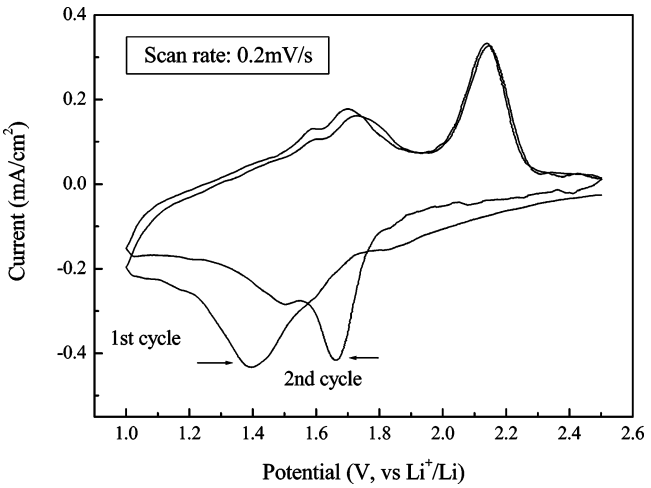

Figure 4. Cyclic voltammograms of electrode made by the anatase nanorods.

Figure 4 shows the cyclic voltammograms (CVs) of electrode made of the anatase nanorods. In the first cycle, one cathodic (insertion) peak of lithium can be found in the voltammograms near 1.39 V vs Li^+/Li; meanwhile, three anodic (extraction) peaks of lithium located at 1.59, 1.73, and 2.14 V vs Li^+/Li were observed, respectively. In the second cycle, however, shifts of peak potentials of cathodic and anodic directions are observed. The dramatic change occurred during the cathodic process. The peak potential of 1.40 V in the first cycle shifts to positive potential and divides into two peak potentials of 1.50 and 1.66 V in the second cycle. The pair of cathodic/anodic peaks at 1.66 and 2.14 V (the actual peak potentials depend on the scan rate) is in accordance with the anatase electrode.[22] On the contrary, the anodic peak potentials move slightly to lower

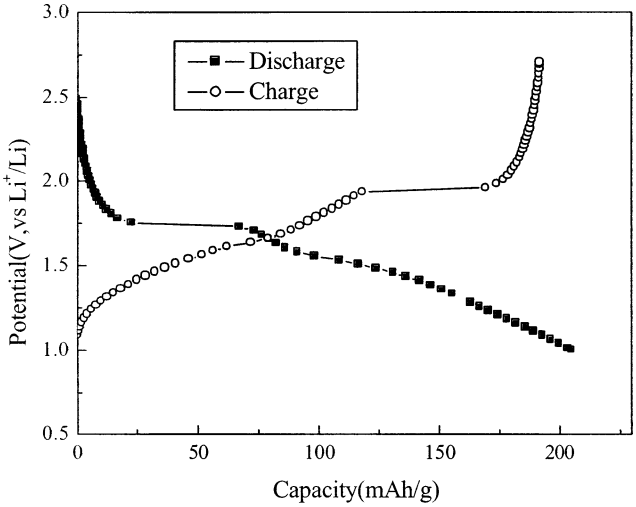

Figure 5. The initial charge−discharge curve of the electrode made by the anatase nanorods at discharge−charge current density of 50 mAh/g at 20 °C.

potentials in comparison with the above two cycles. In the following cycle, the peak potentials and curve shape remain virtually unchanged, being similar to that of the second cycle. Usually, a single cathodic and single anodic peak corresponding to lithium insertion and extraction are observed in spinel, anatase, and rutile.[22] The three pairs of cathodic and anodic peaks were found in the thin layer electrode of highly organized nanotextured anatase[23] owing to the availability of additional sites for lithium insertion and extraction. The splitting and multi peaks associated with differing site occupations are ascribed to the formation of the discrete phase[24] or imperfection of the TiO_2 nanorod lattice, which facilitate the transport of lithium through surface defects and in bulk materials.

Figure 5 displays the initial discharge−charge curves of the electrode made of the anatase nanorods at the current density of 50 mA/g. The initial discharge and charge capacity of the electrode was 206 and 192 mAh/g, respectively, indicating a reversible efficiency as high as 93% for lithium insertion and extraction in the initial discharge−charge curves. There are clear potential plateaus at/near 1.75 and 1.95 V for discharging (insertion of lithium) and charging (extraction of lithium), respectively, which are consistent with the presence of predominantly anatase as the starting material.[25,26] There are also inclined stages of the potentials found at both the ending stage of discharging and initial stage of charging. The two stages correspond to two lithium insertion and extraction steps, which are consisted with the above CVs. The lithium concentration in the lithium titanate phase can be increase up to ~0.6 (Li_x-TiO_2) for chemical intercalation in TiO_2 anatase with *n*-butyllithium.[27] The maximum extraction coefficient of lithium in TiO_2 nanorods is calculated to be 0.6 from electrochemical charge capacity of 192 mAh/g, larger than 0.5 in ordinary anatase[23] and film anatase[28] because only every second oxygen octahedron is occupied by Li due to Li^+-Li^+ Coulomb repulsion.[29] At the surface, however, there possibly exist Li^+ ions in neighboring octahedrons because there the Coulomb interaction may be lower, which could result in a local concentration close to 1, i.e., a higher effective capacity.[29] Surface/bulk ratio for unit cells is estimated as about 1/5 for the nanorods with a diameter of 9 nm. So following that line, ~20% of unit cells at the surface with $LiTiO_2$ instead of $Li_{0.5}$-TiO_2 may explain the higher storage capacity with respect to bulk anatase. The interaction of nanorods with lithium ions occurred mostly at the surface rather than bulk due to the decrease in crystal size,[23] which means that the lithium insertion/extraction could be readily achieved in the TiO_2 nanorods.

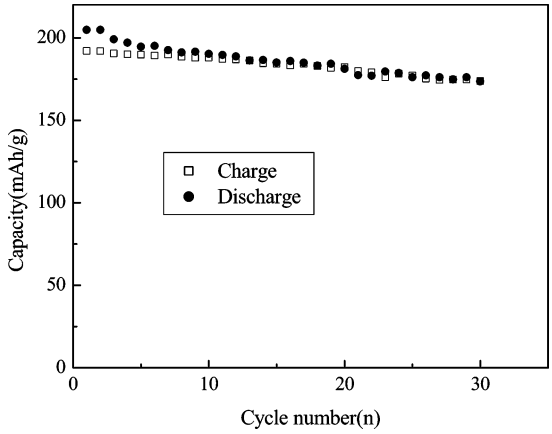

Figure 6. Cycle life of the electrode made by the anatase nanorods at discharge−charge current density of 50 mAh/g at 20 °C.

Cycle behavior of the electrode made of the anatase nanorods under discharge−charge current density of 50 mA/g at 20 °C is depicted in Figure 6. The cutoff potentials for charge and discharge were set to be 2.5 and 1.0 V vs Li^+/Li, respectively. The electrochemical charge−discharge capacity matches each other very well during cycling, revealing a good reversibility of lithium insertion and extraction. It is also observed that the electrochemical capacity decreases gradually to 174 mAh/g after 30 cycles. The optimum cycling behavior was obtained for regimes involving compositions between 0.15 and 0.45 Li/TiO_2 mole ratio as reported previously.[26] Progressive lithium insertion in TiO_2 anatase leads to an increase of lithium titanate phase fraction and a decrease of the lithium anatase phase fraction. However, the lattice volume increases only by about 3%.[29] In addition, a zero-strain insertion reaction without a noticeable change in lattice dimension was demonstrated for Li−Ti−O material.[30] Further improvement of the electrode stability of the TiO_2 nanorods under the large depth of charge−discharge will be an important issue in the future.

IV. Conclusion

In conclusion, the titanate nanorods with a large specific surface area, large pore volume and a diameter of ca. 3−5 nm were initially prepared through NaOH treatment by using $TiCl_4$ as a starting material. The nanorods were converted into nanorods of anatase polycrystalline by a 3 h-calcination at 400 °C, according to the XRD analysis, SAED pattern, and Raman spectra. The anatase nanorods exhibit a high initial capacity and good reversibility for electrochemical lithium insertion. The splitting and multi peaks associated with differing site occupations are ascribed to the formation of the imperfection of the TiO_2 nanorod lattice, which facilitates the transport of lithium through surface defect and in bulk materials.

Acknowledgment. This work is supported by the 973 Program (2002CB211800), the National Key Program for Basic Research (2001CCA05000), the Key Project of Chinese Ministry of Education (03047), the RFDP (20020055007) and NSFC (90206043) of China. Financial supports from the Australian Research Council (ARC) are also gratefully acknowledged and H. Y. Zhu is indebted to ARC for the QE II fellowship.

References and Notes

(1) Kavan, L.; Grätzel, M. *Electrochem. Solid-State Lett.* **2002**, *5* (2) A39−A42.

(2) Wagemaker, M.; Kentgens, A. P. M.; Mulder, F. M. *Nature* **2002**, *418*, 397−399.
(3) Khan, S. U. M.; Shahry, M. A.; Ingler, W. B., Jr. *Science* **2002**, *297*, 2243−2245.
(4) *Handbook of Nanophase and Nanostructured Materials*; Wang, Z.-L., Liu, Y., Zhang, Z., Eds.; Kluwer Academic/Plenum Publishers: New York, 2002; Vol. 1, p 12.
(5) Yuan, Z. Y.; Colomer, J. F.; Su, B. L. *Chem. Phys. Lett*. **2002**, *363*, 362−366.
(6) Zhang, X. Y.; Yao, B. D.; Zhao, L. X.; Liang, C. H.; Zhang, L. D.; Mao, Y. Q. *J. Electrochem. Soc*. **2001**, *148* (7), G398−G340.
(7) Kasuga, T.; Hiramatsu, M.; Hoson, A.; Sekino, T.; Niihara, K. *Langmuir* **1998**, *14*, 3160−3163.
(8) Zhang, S. L.; Zhou, J. F.; Zhang, Z. J.; Du, Z. L.; Vorontsov, A. V.; Jin, Z. S. *Chin. Sci. Bull*. **2000**, *4*5, 1533−1536.
(9) Imai, H.; Takei, Y.; Shimizu, K.; Matsuda, M.; Hirashima, H. *J. Mater. Chem*. **1999**, *9*, 2971−2972.
(10) Kasuga, T.; Hiramatsu, M.; Hoson, A.; Sekino, T.; Niihara, K. *Adv. Mater*. **1999**, *11* (15), 1307−1311.
(11) Wang, Y. Q.; Hu, G. Q.; Duan, X. F.; Sun, H. L.; Xue, Q. K. *Chem. Phys. Lett*. **2002**, *365*, 427−431.
(12) Sasaki, T.; Watanabe, M. *J. Am. Chem. Soc*. **1998**, *120*, 4682−4689.
(13) Ovenstone, J.; Yanagisawa, K. *Chem. Mater*. **1999**, *11*, 2770−2774.
(14) Marchand, R.; Brohan, L.; Tournoux, M. *Mater. Res. Bull*. **1980**, *15*, 1129−1133.
(15) Hu, L.; Tsai, H. L.; Huang, C. L. *J. Eur.. Ceram Soc*. **2003**, *23*, 691.
(16) Yanagisawa, K.; Ovenstone J. *J. Phys. Chem. B* **1999**, *103*, 7781.
(17) Sun, X. M.; Li, Y. D. *Chem. Eur. J*. **2003**, *9*, 2229−2238.
(18) Chen, Q.; Du, G. H.; Zhang, S.; Peng, L. M. *Acta Crystallogr. B* **2002**, *58*, 587−593.
(19) Pottier, A.; Chaneac, C.; Tronc, E.; Mazerolles, L.; Jolivet, J. P. *J. Mater. Chem*. **2001**, *11*, 1116−1121.
(20) Hoyer, P. *Langmuir* **1996**, *12*, 1411−1413.
(21) Yao, B. D.; Chan, Y. F.; Zhang, X. Y.; Zhang, W. F.; Yang, Z. Y.; Wang, N. *Appl. Phys. Lett*. **2003**, *82*, 281−283.
(22) Krtil, P.; Fattakhova, D. *J. Electrochem. Soc*. **2001**, *148* (9) A1045−A1050.
(23) Kavan, L.; Rathousky, J.; Gratzel, M.; Shklover, V.; Zukal, A. *J. Phys. Chem. B* **2000**, *104*, 12012−12020.
(24) Gover, R. K. B.; Tolchard, J. R.; Tukamoto, H.; Murai, T.; Irvinea, J. T. S. *J. Electrochem. Soc*. **1999**, *146* (12) 4348−4353.
(25) Huang, S. Y.; Kavan, L.; Exnar, I.; Gratzel, M. *J. Electrochem. Soc*. **1995**, *142* (9), L142−L143.
(26) Bonino, F.; Busani, L.; Lazzari, M.; Manstretta M.; Rivolta, B.; Scrosati B. *J. Power Sources* **1981**, *6* (3), 261−270.
(27) Wittingham, M. S.; Dines, M. B. *J. Electrochem. Soc*. **1977**, *124*, 1387−1388.
(28) Henningsson, A.; Andersson, M. P.; Uvdal, P.; Siegbahn, H.; Sandell A. *Chem. Phys. Lett*. **2002**, *360* (1−2), 85−90.
(29) Wagemaker, M.; Kearley, G. J.; Well, A. A. van; Mutka, H.; Mulder, F. M. *J. Am. Chem. Soc*. **2003**, *125*, 840−848.
(30) Ohzumu, T.; Ueda, A.; Yamamoto, N. *J. Electrochem. Soc*. **1995**, *1142*, 1431−1435.